PHYSICAL REVIEW FLUIDS **2**, 032602(R) (2017)

Jets or vortices—What flows are generated by an inverse turbulent cascade?

Anna Frishman,[1,2] Jason Laurie,[1,3] and Gregory Falkovich[1,4]
[1]*Department of Physics of Complex Systems, Weizmann Institute of Science, Rehovot 76100, Israel*
[2]*Princeton Center for Theoretical Science, Princeton University, Princeton, New Jersey 08544, USA*
[3]*Mathematics Group, School of Engineering and Applied Science, Aston University, Birmingham B4 7ET, United Kingdom*
[4]*Institute for Information Transmission Problems, Moscow 127994, Russia*
(Received 15 August 2016; published 29 March 2017)

An inverse cascade, energy transfer to progressively larger scales, is a salient feature of two-dimensional turbulence. If the cascade reaches the system scale, it creates a coherent flow expected to have the largest available scale and conform with the symmetries of the domain. In a doubly periodic rectangle, the mean flow with zero total momentum was therefore believed to be unidirectional, with two jets along the short side; while for an aspect ratio close to unity, a vortex dipole is expected. Using direct numerical simulations, we show that in fact neither is the box symmetry respected nor the largest scale realized: the flow is never purely unidirectional since the inverse cascade produces coherent vortices, whose number and relative motion are determined by the aspect ratio. This spontaneous symmetry breaking is closely related to the hierarchy of averaging times. Long-time averaging restores translational invariance due to vortex wandering along one direction, and gives jets whose profile, however, can neither be deduced from the largest-available-scale argument, nor from the often employed maximum-entropy principle or quasilinear approximation.

DOI: 10.1103/PhysRevFluids.2.032602

Introduction. An inverse cascade is a counterintuitive process of self-organization of two-dimensional turbulence. In an infinite medium, the cascade creates vortices (vortex rings in curved space [1]) of ever-increasing size, while in a finite domain it eventually forms a flow coherent in the entire system. That flow is expected to become universal, i.e., independent of the forcing, when the forcing scale goes to zero, keeping the energy input rate finite. Predicting the form of the flow in various settings is one of the central problems of turbulence theory. There are three known approaches to address this issue. The first way is qualitative: to look for the flow with the largest available scale (e.g., a flow dominated by the Fourier modes with the smallest wave number). A quantitative way, a statistical equilibrium theory, considers a flow profile that maximizes entropy for a given vorticity distribution and energy [2,3]. It is strictly applicable only in the absence of forcing, although deviations from the predictions have been observed even then (see, e.g., [4–8]). The third approach is to assume that turbulence is weak relative to the mean flow and employ a quasilinear approximation; writing equations for the two-point correlation functions (of velocity or vorticity) to form a closed system [9–12], or using a single-point reduced description of spatial fluxes (of energy, momentum, enstrophy) [13,14]. The limitations of the quasilinear approximation for atmospheric flows have been pointed out in [15].

Perhaps the simplest setting is a rectangle with periodic boundary conditions (a torus). The system is translation invariant along x and y; any nonuniform mean flow breaks one of these symmetries or both. Flow on a torus may have either contractible streamlines corresponding to vortices or noncontractible streamlines corresponding to jets. Jets going around one side may be expected in a (nonsquare) rectangle where there is no symmetry between directions. Indeed, a maximal-entropy analysis [16], predicts two opposing jets (for zero total momentum) directed along the shorter side of the domain for large enough aspect ratios. The nonequilibrium steady state was analyzed numerically in [16] and compared to this prediction. It was asserted that the mean flow indeed transitions between two jets consisting solely of noncontractible loops for a rectangle, and a vortex dipole, containing contractible streamlines, for domains close to a square.

One may also try to explain the appearance of the two flow types via the largest scale argument: for an aspect ratio l_x substantially different from one, the largest mode is two opposite jets along the short side. On the other hand, in a square box, the jets can be directed along either side and one may expect a superposition of two sets of jets, which would look like a vortex dipole [16,17]. In this picture, jets are fundamental objects on a torus while the vortex dipole appears only near a degeneracy, when $l_x \approx 1$.

In fact, the vortex, created by an extended inverse cascade in a square box of size $L \times L$, cannot be represented as a superposition of jets [13,18], since the analysis of spatial fluxes of energy and momentum gives the velocity profile $U(r) \propto$ const at the distance from the vortex center $r \ll L$ [13]; that corresponds to the stream function $\psi(r) \propto r$ which cannot be represented as a superposition of orthogonal jets, $\psi(x,y) = \phi(x) + \phi(y)$.

In the present work, we focus on the universal limit of small-scale forcing and the culmination of an extended inverse cascade in a rectangle. Our numerical modeling reveals how all the expectations are defied by nature: there is no dichotomy between vortices and jets, which coexist for any aspect ratio. In fact, such vortices also appeared in [16], but were interpreted as intermediate size fluctuations rather than as part of the mean flow [17]. For domains with a moderate l_x, we find two jets and a vortex dipole at zero-velocity streamlines. When averaged over the shortest dynamical time scale, the mean flow seems to be close to a steady Euler solution (compare Fig. 2 and Fig. S3 in the Supplemental Material [19]). On longer time scales, the distance between the vortices in the dipole varies, due to the influence of both fluctuations and jets. The asymptotic state is sensitive to the value of very small uniform friction: as it decreases for a moderate l_x, an additional vortex, which can be of either sign, emerges. Then, the two same-sign vortices no longer lie directly between the two jets, but inside opposing jets, giving a nonzero mean velocity, which implies the flow cannot correspond to a steady Euler solution. When the dipole or the three-vortex flow is averaged over long times, vortices are smeared into stripes, resulting in a two-jet mean flow. Decreasing the aspect ratio even further causes the appearance of additional vortices, and what is more interesting, additional jets, which persist under long-time averaging. We thus find that the first two approaches (largest-scale and maximal-entropy), to the extent they can be applied, give incorrect predictions. The third approach, the quasilinear approximation, relies on the expectation that the mean flow will dominate over turbulent fluctuations. It requires a proper account of the flow geometry and averaging time, and correctly describes the interior of a circular vortex [13], but fails to describe the global mean flow in a rectangle: the zonal or long-time average treats vortices as fluctuations making the latter strong, as our numerics show. Our work thus demonstrates that the principles of organization of an inverse cascade into a mean flow are currently lacking.

Jets and vortices. We consider an incompressible flow, $\boldsymbol{\nabla} \cdot \mathbf{v} = 0$, described by the two-dimensional Navier-Stokes equations for a fluid with unit density:

$$\partial_t \mathbf{v} + (\mathbf{v} \cdot \boldsymbol{\nabla})\mathbf{v} = -\boldsymbol{\nabla} p - \alpha \mathbf{v} + \nu \nabla^2 \mathbf{v} + \mathbf{f}. \tag{1}$$

The force $\mathbf{f}$ acts in a narrow band of scales $l_f \ll L$. The energy injection rate is $\epsilon = \langle \mathbf{f} \cdot \mathbf{v} \rangle$. We assume that system-size eddies produced by an inverse cascade have turnover times much shorter than the time of frictional dissipation: $\delta \equiv \epsilon^{-1/3} L^{2/3} \alpha \ll 1$. Then the inverse cascade fed by our small-scale forcing reaches the system scale producing energy accumulation and generating a mean flow. In the steady state at high Reynolds number, $\mathrm{Re} = \epsilon^{1/3} l_f^{4/3}/\nu \gg 1$, most of the energy is dissipated by the friction of the mean flow, giving the mean velocity estimate $U \simeq \sqrt{\epsilon/\alpha}$, and the corresponding turnover time $\tau_m = \sqrt{\alpha L^2/\epsilon}$.

We numerically solve (1) in the vorticity formulation in a periodic rectangle of size $2\pi l_x \times 2\pi$ using a $512 l_x \times 512$ grid with uniform spacing in both directions. We implement a pseudospectral method using the 3/2-dealiasing rule and time step using a fourth-order exponential time-difference algorithm. Our stochastic forcing implements the Euler-Maruyama method, where each Fourier mode of the forcing is a complex Gaussian random variable, correlated up to the time step dt of our simulations (see the Supplemental Material), with fixed amplitude equal to 0.1 in an annulus

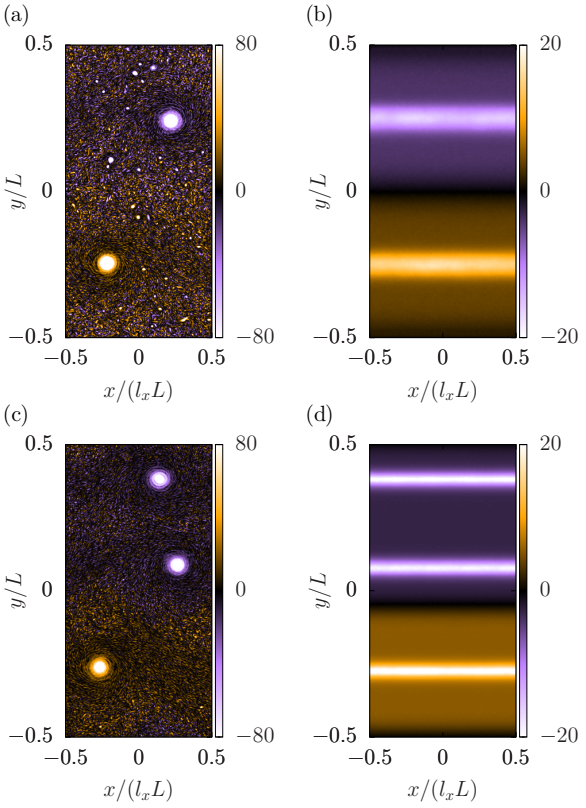

FIG. 1. Scaled total vorticity $\sqrt{\alpha L^2/\epsilon}(\nabla \times \mathbf{v})$ for runs A and F, respectively: (a) and (c) a snapshot; (b) and (d) a temporal average over time $1/\alpha$ with frames shifted to align the velocity maximum with $y = 0$.

of width $99 \leqslant k < 101$ (acting as an approximation to delta-correlated white noise). The forcing scale is defined as $l_f = 2\pi/k_f$ with $k_f \approx 100$. In order to provide as large as possible inertial range for the inverse cascade, we replace regular viscosity with hyperviscosity $-\nu(-\nabla^2)^p\mathbf{v}$ with $p = 8$ and $\nu = 1 \times 10^{-36}$. Each simulation is run so that a statistical steady state is reached, verified by monitoring the total energy. We compute the energy dissipation rate via friction using it as a measure of the inverse energy flux and an estimate for ϵ. All of our data analysis is performed in the statistical steady state.

We begin from $l_x < 1$ to see if the emergent mean flow has two opposite jets parallel to $\hat{x}$, with all averaged quantities independent of x. We perform three simulations, denoted by A–C, with $\alpha = 1 \times 10^{-4}$ and with different aspect ratios: $l_x = 1/2, \delta = 5.58 \times 10^{-3}$ (A), $l_x = 3/4, \delta = 4.86 \times 10^{-3}$ (B), and $l_x = 1$, $\delta = 4.39 \times 10^{-3}$ (C). The typical vorticity snapshot in a steady state reveals a surprising feature: large-scale coherent vortices in addition to jets [see Fig. 1(a)]. Considering the dynamical generation of the mean flow, the presence of vortices is natural: locally the inverse cascade tends to create vortices, and the anisotropy of the box is felt only when their size is comparable to $l_x L$. Once established, the opposite-signed vortices feed on the constantly created smaller vortices, counteracting the effect of dissipation.

Any meaningful discussion of the emerging mean flow and symmetries must address the averaging times. For $t \lesssim \tau_m$ the centers of the vortices are effectively pinned. Averaging on such time scales, the mean flow can be characterized by streamlines as presented in Fig. 2. Topologically, the mean flow consists of two distinct regions of contractible streamlines surrounding the centers of the two vortices. In between the two regions, a separatrix should be present. The positive vortex is at $(-l_x L/4, -L/4)$ in Fig. 2. The symmetry of the streamline pattern around the vortex center dictates that the separatrix

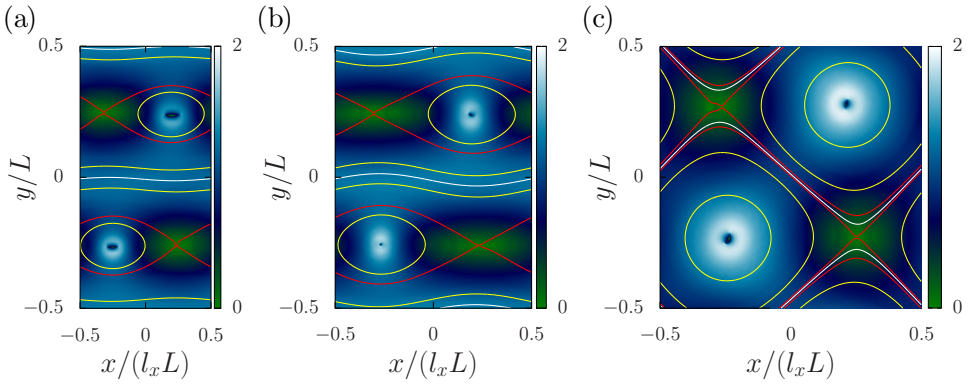

FIG. 2. Heat maps of the scaled speed ($\sqrt{\alpha/\epsilon}|\mathbf{v}|$) averaged over time τ_m: (a) run A, (b) run B, and (c) run C. Overlaid are streamlines, red lines are separatrices, and white lines correspond to $\psi = 0$.

would pass through $(l_x L/4, -L/4)$, which is a stagnation point due to periodicity. For a square box, the vortices are arranged in a diagonal lattice, with the second vortex located at $(l_x L/4, L/4)$ and the separatrix passing through the stagnation point $(-l_x L/4, L/4)$. A separatrix composed of two straight streamlines connecting the two stagnation points preserves the x-y symmetry, and is therefore expected for a square box where $l_x = 1$. For $l_x < 1$, this symmetry is absent and there is no reason for the two stagnation points to lie on the same streamline. We thus expect the separatrix to split into two, giving rise to two regions of noncontractible streamlines, i.e., jets. We indeed observe this splitting for aspect ratios $1/2$ and $3/4$, as seen in Fig. 2. In the square box, we also find the x-y symmetry spontaneously broken by a tiny splitting of the separatrix, creating an opening for weak jets.

On larger time scales, associated to the fluctuations $t \gtrsim \tau_f \equiv \epsilon^{-1/3} L^{2/3}$, a collective motion of the vortices, and a relative horizontal motion for $l_x < 1$, becomes appreciable (see Fig. 3 and Fig. S4 in the Supplemental Material]. In particular, for $l_x = 1/2$ and $l_x = 3/4$, the diagonal lattice is only one among a continuum of possible configurations. In a square box, on the other hand, the vortices are almost completely restricted to the diagonal, separated by the maximal possible distance $L/\sqrt{2}$. This hints at the existence of a minimal distance between the vortex centers, which prevents the two vortices from approaching closer, dictating the extent of their relative motion. The fact that the vortices remain at the distance $L/\sqrt{2}$ for a square box suggests the guess that $l_x L/\sqrt{2}$ is the minimal vortex separation for an arbitrary aspect ratio l_x. Correspondingly, we find that the extent

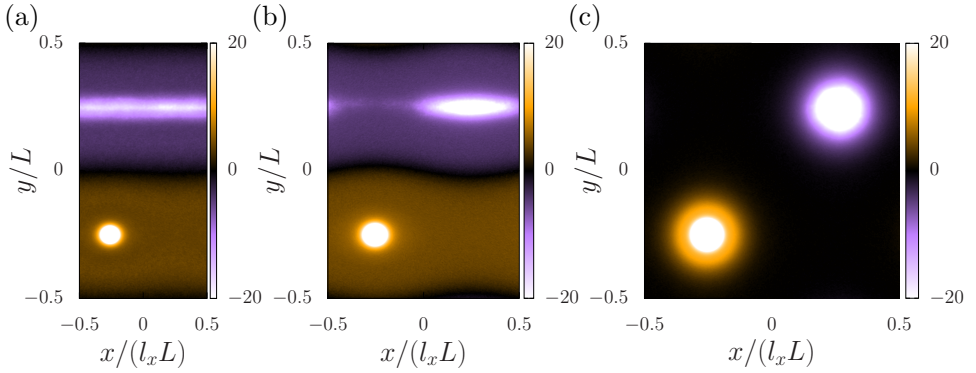

FIG. 3. Scaled total vorticity $\sqrt{\alpha L^2/\epsilon}(\nabla \times \mathbf{v})$ averaged over time $1/\alpha$ in the reference frame of the positive vortex: (a) run A, (b) run B, and (c) run C.

of the horizontal relative motion of the vortices for $l_x = 3/4$ is close to $(l_x - \sqrt{2l_x^2 - 1})L$ [see Fig. 3(b); see also Fig. S1 in the Supplemental Material]. This is in agreement with the absence of configurations with inter-vortex separations smaller than $l_x L/\sqrt{2}$, assuming that the vertical relative motion is negligible. Under the same assumption, the full extent of the relative horizontal motion should become possible for aspect ratios $l_x < 1/\sqrt{2}$. Indeed, as observed in Fig. 3(a) for $l_x = 1/2 < 1/\sqrt{2}$, the second vortex explores the line $y = L/4$ with equal probability.

For $l_x = 1/2$, we performed simulations for different δ: $\delta = 1.12 \times 10^{-2}$ (D), $\delta = 2.78 \times 10^{-3}$ (E), and $\delta = 1.67 \times 10^{-3}$ (F). Astonishingly, the vortex dipole of simulations A and D is replaced by a three-vortex configuration for the low-friction simulations E and F [see Fig. 1(a)]. In this configuration, the two same-sign vortices lie inside different jets, moving horizontally in opposite directions already on time scales of order τ_m. The third vortex remains on the zero-velocity line between two jets. The distance between the opposite-sign vortices always exceeds the suggested minimal distance, $l_x L/\sqrt{2}$. In [20], it was argued that the size of the vortices should grow with decreasing δ for fixed l_f and ϵ; this contradicts the appearance of additional vortices found here.

How many vortices does the asymptotic $\delta \to 0$ state contain for a given l_x? If indeed there exists a minimal sustainable separation between opposite-sign vortices, then their number is limited by it. Assuming adjacent same-signed vortices can appear only inside different jets, then at most four vortices, arranged in a diagonal lattice, can be present for $l_x = 1/2$. The emergence of such a constricted arrangement out of the three-vortex configuration seems improbable. Thus, three vortices may be the asymptotic state for $l_x = 1/2$.

Simulations G and H were performed, for $l_x = 1/3$, $\delta = 6.22 \times 10^{-3}$ and $l_x = 1/4$, $\delta = 6.83 \times 10^{-3}$ respectively. With decreasing aspect ratio, not only does the number of vortices increase but also the number of jets: four jets are present for $l_x = 1/4$. This implies that the length of the short side of the box plays a crucial role in determining the jets, in contradiction to the largest-mode argument. Snapshots of the vorticity field are presented in Fig. S6 of the Supplemental Material.

Long-time average: Mean flow and fluctuations. In the limit $\delta \to 0$, τ_m and $\tau_d \equiv 1/\alpha$ become well separated and one can average over a time between them. For $l_x < 1$, while there is random motion along x on such time scales, almost no vertical (collective or relative) motion of the vortices is observable even for the longest times of order τ_d, on which the square-box mean flow is close to zero (see Fig S5 in the Supplemental Material). Thus, averaging over $t \gg \tau_f \gg \tau_m$ smears vortices into stripes resulting in an effective jet-like mean flow homogeneous in x, as is shown in Figs. 1(b) and 1(d) for $l_x = 1/2$ (the relevance of such a situation for the ocean was suggested in [21]). In Figs. 1(b) and 1(d) we align frames by the line of maximum (positive) x-averaged velocity. While the size of the vortices only slightly decreases with δ (see Fig. 1), the averaged vorticity strip is narrower for smaller δ due to the suppression of the fluctuations which cause the vertical drift of the vortices.

The statistical homogeneity along x at long times allows for an analysis of the energy and momentum balance similar to that in [13]. Accordingly, we decompose the velocity into its mean $U(y)$ and fluctuating components: $\mathbf{v} = (u + U, v)$ where u and v are the corresponding fluctuating velocity fields in the x and y directions, and $\langle u \rangle = \langle v \rangle = 0$, the average being over time. In the simulations a zonal average along x is added. We write the steady-state conservation of the x momentum and energy neglecting the viscous terms, assuming $\nu/\alpha L^2 \ll 1$ and $\mathrm{Re} \to \infty$. Denoting y derivatives by a prime, one gets

$$\partial_y \langle uv \rangle + \alpha U = 0, \tag{2}$$

$$\partial_y \left\langle v \left(p + \frac{u^2 + v^2}{2} \right) \right\rangle = \epsilon - U' \langle uv \rangle - \alpha \langle u^2 + v^2 \rangle. \tag{3}$$

To make analytical progress, one usually assumes that fluctuations are suppressed by the mean flow and employs the quasilinear approximation, neglecting the cubic terms in Eq. (3). The assumption seems to be supported both by the energy argument (most of the energy is transferred from

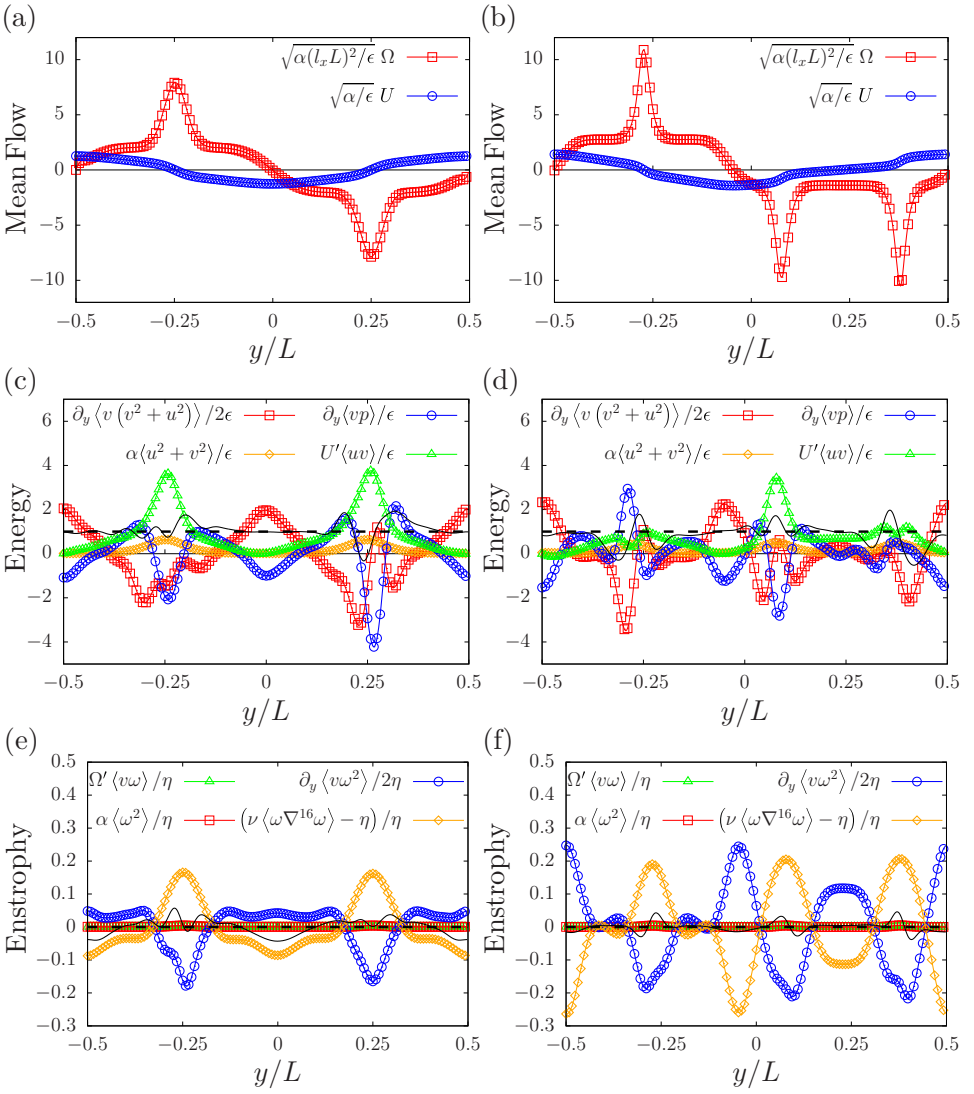

FIG. 4. Mean profiles of vorticity and velocity (top), balances of energy (middle), and enstrophy (bottom) for run A (right) and run F (left). Horizontal dashed lines indicate the expected balance; solid lines indicate the numerical sum. Data were averaged over time exceeding τ_d with frames shifted to align the velocity maximum with $y = 0$.

fluctuations to the mean flow so one expects interactions of fluctuations to be unimportant) and by the momentum balance in Eq. (2) which gives $\langle uv\rangle \simeq \sqrt{\delta}(\epsilon L)^{2/3}$. For a circular vortex it was assumed additionally that the whole energy flux divergence is negligible [13], including the pressure term. Using this assumption, Eq. (3) is reduced to $\epsilon = U'\langle uv\rangle$, resulting in a closed system for $\langle uv\rangle$ and U as $\delta \to 0$. Jets, however, have lines with $U' = 0$, where we expect the energy flux divergence to be comparable to ϵ.

Figures 4(a) and 4(b) show the mean flow profiles for simulations A and F, and Figs. 4(c) and 4(d) present the terms of (3). To reduce noise, the data were low-pass filtered using a Gaussian kernel in Fourier space with an effective cutoff $L/8$. Under long-time (or zonal) averaging, the vortices contribute to both the mean flow and the fluctuations, making them strong. The locations of the vortices are thus characterized by peaks in the energy dissipation of the fluctuations.

For the dipole, the energy flux divergence is important everywhere, and in particular the cubic terms are not small. The flow thus cannot be described by a quasilinear approximation anywhere. In the three-vortex configuration, simulation F, the energy flux divergence is negligible in a small region between the same-sign vortices; the approximation of [13] seems to be applicable there. The black curve in Figs. 4(c) and 4(d), representing the sum of terms in (3) without ϵ, shows convergence of the statistics. Naturally, it is worse in the region of vortices where fluctuations are stronger.

It is also illuminating to consider the balance of enstrophy (squared vorticity) for the fluctuations:

$$\tfrac{1}{2}\partial_y\langle v\omega^2\rangle = Q - \langle v\omega\rangle\Omega', \tag{4}$$

where ω and $\Omega = -U'$ are the fluctuating and mean vorticity, respectively, and $Q = \eta - \nu\langle\omega(-\nabla^2)^p\omega\rangle - \alpha\langle\omega^2\rangle$ with $\eta = \langle\omega(\boldsymbol{\nabla}\times\mathbf{f})\cdot\hat{z}\rangle$. Most of the injected enstrophy should be dissipated in the direct cascade by viscosity, so that when integrated over y, Q is a small but finite rate of enstrophy absorption by the mean flow. The turbulence-flow enstrophy exchange term, $\langle v\omega\rangle\Omega' = \alpha U\Omega'$, turns into zero where $\Omega' = 0$ and $U = 0$. That hints that the cubic term (turbulent enstrophy flux divergence) may be large there and the quasilinear approximation invalid. Indeed, we find in Figs. 4(e) and (f) that the enstrophy balance is everywhere dominated by Q and the turbulent flux, which goes from the jets to vortices, where viscous dissipation is larger. The quasilinear approximation thus fails even in the regions where the velocity cubic terms are small in Figs. 4(c) and 4(d).

To conclude, let us reiterate the hierarchy of fluctuations and symmetries. The cascade-related weak fluctuations with velocities $v_f \simeq (\epsilon L)^{1/3}$ average to zero on a time scale exceeding their correlation time $\tau_f = L/v_f$. Vortices and jets have much larger velocities $U \simeq \sqrt{\epsilon/\alpha}$ and persist in the steady state. Fluctuations make the vortices wander along the jets, so averaging in a fixed reference frame over times exceeding τ_f (and hence exceeding their turnover time L/U) makes the flow unidirectional and restores the translation invariance along the short direction x. One may expect that averaging over even longer time scales gives zero mean flow and thus restores translational invariance along both x and y. However, we found such a time only for a square box where the vortex dipole wanders around because the distance between vortices fluctuates. In the rectangle, the longest averages (over times exceeding $1/\alpha$) give stable jets and thus do not restore the translation invariance along y. Apparently, it is much easier to move vortices or dipoles than it is to shift jets. Note also the remarkable breakdown of reflection symmetry by the appearance of a third vortex at lower friction.

This work provides only a first glimpse into the intricacies of flows created by an inverse cascade in a box with a globally broken x-y symmetry. In geophysical systems one also has differential rotation (β effect), which breaks the symmetry locally and is expected to destroy the large-scale vortices. We leave the complete characterization of the parameter space δ,l_x,β for a future publication.

Acknowledgments. The authors are grateful to T. Grafke, V. Lebedev, and P. Wiegmann for illuminating discussions. A.F. was supported by the Adams Fellowship Program of the Israel Academy of Sciences and Humanities. The work of G.F. was supported by Grant No. 882 of the Israel Science Foundation and project 14-22-00259 of the Russian Science Foundation.

A.F. and J.L. contributed equally to this work.

[1] Gregory Falkovich and Krzysztof Gawedzki, Turbulence on hyperbolic plane: The fate of inverse cascade, J. Stat. Phys. **156**, 10 (2014).

[2] Jonathan Miller, Statistical Mechanics of Euler Equations in Two Dimensions, Phys. Rev. Lett. **65**, 2137 (1990).

[3] R. Robert and J. Sommeria, Statistical equilibrium states for two-dimensional flows, J. Fluid Mech. **229**, 291 (1991).

[4] A. Venaille, T. Dauxois, and S. Ruffo, Violent relaxation in two-dimensional flows with varying interaction range, Phys. Rev. E **92**, 011001 (2015).

[5] David G. Dritschel, Wanming Qi, and J. B. Marston, On the late-time behavior of a bounded, inviscid two-dimensional flow, J. Fluid Mech. **783**, 1 (2015).
[6] Shun Ogawa, Julien Barré, Hidetoshi Morita, and Yoshiyuki Y. Yamaguchi, Dynamical pattern formation in two-dimensional fluids and Landau pole bifurcation, Phys. Rev. E **89**, 063007 (2014).
[7] Hidetoshi Morita, Collective oscillation in two-dimensional fluid, arXiv:1103.1140.
[8] Patrick Tabeling, Two-dimensional turbulence: A physicist approach, Phys. Rep. **362**, 1 (2002).
[9] Brian F. Farrell and Petros J. Ioannou, Structure and spacing of jets in barotropic turbulence, J. Atmos. Sci. **64**, 3652 (2007).
[10] Kaushik Srinivasan and W. R. Young, Zonostrophic instability, J. Atmos. Sci. **69**, 1633 (2011).
[11] S. M. Tobias, K. Dagon, and J. B. Marston, Astrophysical fluid dynamics via direct statistical simulation, Astrophys. J. **727**, 127 (2011).
[12] F. Bouchet, C. Nardini, and T. Tangarife, Stochastic averaging, large deviations and random transitions for the dynamics of 2D and geostrophic turbulent vortices, Fluid Dyn. Res. **46**, 061416 (2014).
[13] Jason Laurie, Guido Boffetta, Gregory Falkovich, Igor Kolokolov, and Vladimir Lebedev, Universal Profile of the Vortex Condensate in Two-Dimensional Turbulence, Phys. Rev. Lett. **113**, 254503 (2014).
[14] Gregory Falkovich, Interaction between mean flow and turbulence in two dimensions, Proc. R. Soc. A **472**, 20160287 (2016).
[15] S. M. Tobias and J. B. Marston, Direct Statistical Simulation of Out-of-Equilibrium Jets, Phys. Rev. Lett. **110**, 104502 (2013).
[16] Freddy Bouchet and Eric Simonnet, Random Changes of Flow Topology in Two-Dimensional and Geophysical Turbulence, Phys. Rev. Lett. **102**, 094504 (2009).
[17] Freddy Bouchet and Antoine Venaille, Statistical mechanics of two-dimensional and geophysical flows, Phys. Rep. **515**, 227 (2012).
[18] M. Chertkov, C. Connaughton, I. Kolokolov, and V. Lebedev, Dynamics of Energy Condensation in Two-Dimensional Turbulence, Phys. Rev. Lett. **99**, 084501 (2007).
[19] See Supplemental Material at http://link.aps.org/supplemental/10.1103/PhysRevFluids.2.032602 for details about the numerical scheme and the parameters used; a plot of the probability density function for the relative x separation between vortices in simulations A-C, compared to the crude prediction in the main text; plots of vorticity averaged over the various time scales in the problem, performed in a fixed reference frame; a plot of the vorticity snapshot for domain aspect ratios $1/3$ and $1/4$, showing the appearance of multiple jets and vortices; and plots of the energy spectrum for the simulations, demonstrating that they are sufficiently resolved.
[20] I. V. Kolokolov and V. V. Lebedev, Structure of coherent vortices generated by the inverse cascade of two-dimensional turbulence in a finite box, Phys. Rev. E **93**, 033104 (2016).
[21] Michael G. Schlax and Dudley B. Chelton, The influence of mesoscale eddies on the detection of quasi-zonal jets in the ocean, Geophys. Res. Lett. **35**, L24602 (2008).